Catalysis Science & Technology

Accepted Manuscript

ROYAL SOCIETY OF CHEMISTRY

www.rsc.org/catalysis

Journal Name

ARTICLE

Identifying Descriptor of Governing NO Oxidation on Mullite Sm(Y, Tb, Gd, Lu)Mn_2O_5 for Diesel Exhaust Cleaning†

Received 00th January 20xx,
Accepted 00th January 20xx

DOI: 10.1039/x0xx00000x

www.rsc.org/

Hao-Bo Li,[a] Wei-Hua Wang,[a] Xinyu Qian,[a] Yahui Cheng,[a] Xinjian Xie,[b] Jieyu Liu,[a] Shuhui Sun,[c] Jigang Zhou,[d] Yongfeng Hu,[d] Jianping Xu,[e] Lan Li,[e] Yan Zhang,[f] Xiwen Du,[f] Kuanghong Gao,[g] Zhiqing Li,[g] Cui Zhang,[h] Shudong Wang,[i] Haijun Chen,[i] Yidong Zhao,[j] Feng Lu,[a*] Weichao Wang,[a*] and Hui Liu[a]

The current fast selective catalytic reduction (fast-SCR) technology shows an effectiveness of converting the diesel engine generated nitrogen oxides NO_x to environmentally benign nitrogen (N_2) with the aid of the precious metal catalyst platinum. Driven by previous finding of the low-cost mullite's great superiority over Pt in term of NO oxidation, a series of Mn-based oxides Sm(Y, Tb, Gd, Lu)Mn_2O_5 materials are synthesized to identify a general descriptor to govern the catalytic performance. Utilizing soft X-ray absorption characterization and molecular orbital theory, here, we show that catalytic activity difference presents little dependence on the 3d electron occupancy when varying A site element (Sm, Tb, Y, Gd, Lu). Instead, strong *p-d* hybridization between lattice O and octahedral Mn leads to weak bonding strength between external O* and pyramid Mn and essentially increases the catalytic behavior of converting NO to NO_2.

1 Introduction

The focus on diesel exhaust control has been on emissions of the nitrogen oxides (NO_x) and particulate matter (PM) due to their sizable contribution to global warming and human res- piratory problems .[1,2] Fast selective catalytic reduction (fast-SCR) technology was developed to convert NO_x into N_2 in the presence of excess oxygen, O_2.[3] The chemical principle of fast-SCR is to break down urea to provide ammonia which further reacts with $NO+NO_2+O_2$ and produce water and N_2.[4,5] The NO_x in the diesel exhaust is composed of ~90% NO, it is therefore critical to oxidize NO so that the reduction reaction reaches its maximum rate via fast SCR. So far, precious metal platinum (Pt) is widely used to drive the NO oxidation with a high efficiency (60% at 300 °C).[6] Due to the high price and limited abundance of Pt, it is an ecnomic challenge to implement increasing Pt concentration in diesel after-treatment systems. Thus, catalysts with low cost, greater abundance and high thermal durability for NO oxidation are strongly desirable. A significant amount of work has been undertaken in search for possible catalysts based on transition metal oxides.[7-9] Kim *et al* have synthesized strontium doped perovskites, $La_{0.9}Sr_{0.1}Co(Mn)O_3$, showing superior performance to Pt-based catalyst.[7] In the continuous searching for highly active oxide catalysts, Wang *et al* have recently presented a new class of hydrothermally stable, mixed-phase oxide materials rooted in Mn-mullite AMn_2O_5 (A=Sm,Gd).[10] These mullite oxides demonstrate an activity at temperatures as low as 75 °C and has a ~45% increasein NO oxidation catalytic performance over Pt at 300 °C.

In order to design better catalysts according to current mullite oxides, a catalytic descriptor, i.e. *d*-orbitals related characters determining catalytic NO oxidation, should be urgently identified. Proposed in Nørskov's *d*-band theory, for precious metals *d*-band center basically controls the catalytic activity via bonding strength between the incoming molecules and the precious metal surfaces.[11] The *d*-band theory could be extended to perovskite oxide for oxygen reduction (evolution) reactions, i.e. ORR (OER).[12,13] They discovered that e_g-orbitals filling and the orbitals hybridization between O-2*p* and Mn-3*d* are the key factors to manipulate the catalytic behaviour. Nevertheless, their findings might not be directly applied to the Mn-based mullite oxides stemming from much more complicated crystal structures in which Mn atoms present two different types of Mn-O ligand fields: octahedral (Mn_{oct}) and square pyramid (Mn_{pyr}). Additionally, the physical relationship between the catalytic mechanism and the *p-d* hybridization is still unknown for both Mn-based mullites and perovskites. In our previous work, we proposed the perceptive Mn_{pyr}-Mn_{pyr} dimer as an active site.[10] But, further fundamentally *d*-band

[a] Department of Electronics, Nankai University, 300071, China. E-mail: weichaowang@nankai.edu.cn, lufeng@nankai.edu.cn
[b] School of Materials Science and Engineering Hebei, University of Technology Tianjin, 300401, China
[c] Institut National de la Recherche Scientifique, Que´bec, J3X 1S2, Canada
[d] Canadian Light Source, Saskatoon, S7N 2V3, Canada
[e] College of Science, Tianjin University of Technology, 300384, China
[f] School of Materials Science and Engineering, Tianjin University, 300072, China
[g] Department of Physics, Tianjin University, 300072, China
[h] College of Chemistry, Nankai University, 300071, China.
[i] Dalian Institute of Chemical Physics, Chinese Academy of Sciences, 116023 China
[j] Beijing Synchrotron Radiation Facility, Chinese Academy of Sciences, 100049, China.

†Electronic Supplementary Information (ESI) available: [details of any supplementary information available should be included here]. See DOI: 10.1039/x0xx00000x

Journal Name

ARTICLE

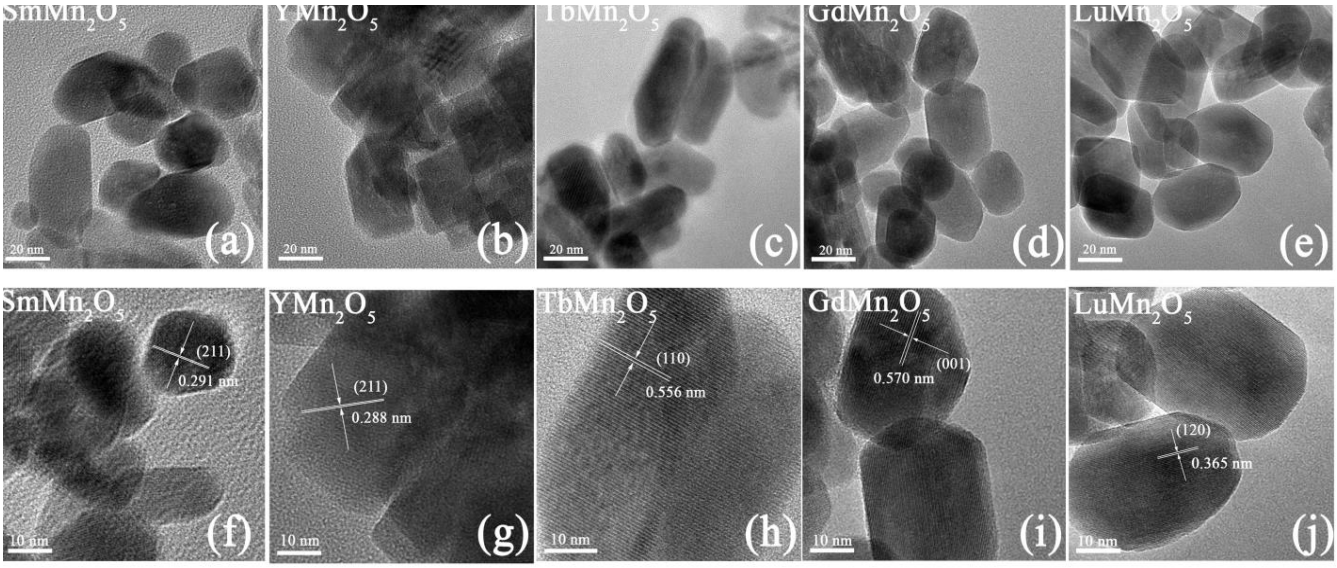

Fig. 1 TEM and HRTEM images. (a-e), The TEM figures of the $SmMn_2O_5$, YMn_2O_5, $TbMn_2O_5$, $GdMn_2O_5$ and $LuMn_2O_5$, respectively. (f-j), The HRTEM images of corresponding nanoparticles.

related general descriptor is not accessible to illustrate the catalytic behaviour. In this work, we combine soft X-ray absorption spectrum (XAS) and density functional theory (DFT) calculations to identify a general descriptor, i.e., *p-d* orbitals hybridization strength between lattice O (O_{bulk}) and the Mn_{oct}, governing NO oxidation on mullite (AMn_2O_5) with a variation of A site elements (Sm, Y, Tb, Gd, Lu). Such intrinsic relationship between fundamental molecular orbitals and catalytic performance provides insights to future rational design oxide-based catalysts.

2 Methods

For our experiments, we prepared the pure mullite powders through hydrothermal methods (See Supplementary Information). The DFT calculation was performed by using Vienna *ab* initio simulation package (VASP). The generalized gradient approximation (GGA) with exchange-correlation function of Perdew, Burke and Ernzerhof (PBE) was chosen.[14] For transition metal Mn, psuedopotential with electron configuration of $3d^6 4s^1$ was chosen. For *f*-elements such as Sm ($4f^6\ 6s^2$), psuedopotential with part of frozen *f*-electrons was selected. For instance, the psuedopotential of Sm^{3+} was generated by keeping 5 *f*-electrons frozen in the core.[15] A (2×4×8) Monkhorst-Pack *k*-point grid was adopted and the energy cutoff was set to be 400 eV. In the structure relaxation, the maximum force on each atom was converged to 0.001 eV/Å. A (2×1×1) unit cell is selected and the collinear spin approximation of the magnetic structure was adopted according to the reference work (See Supplementary Information).[16]

3 Results and discussion

The X-ray diffraction (XRD) spectra confirm the pure mullite crystalline in orthorhombic phases with space group of *Pbam* (See Supplementary Information, Figure S1). The transmission electron microscope (TEM) shows that the nanoparticles shapes are irregular and the average size of the nanoparticles is ~60 nm in all five samples Sm(Y, Tb, Gd, Lu)Mn_2O_5 (Figure1(a-e)). The high-resolution TEM images reveal the lattice plane of (211), (211), (110), (001) and (120) of Sm(Y, Tb, Gd, Lu)Mn_2O_5 nanostructures as labelled in Figure 1(f-j), respectively. Thus the Sm(Y, Tb, Gd, Lu)Mn_2O_5 powder all consists of randomly crystallized nanoparticles without unique morphological properties, which might not cause a major difference in the catalytic efficiency of Sm(Y, Tb, Gd, Lu)Mn_2O_5. The BET surface area measurement exhibits an average surface area of ~56.9 m^2/g (See Supplementary Information) with a small deviation of 6.34 m^2/g.

The NO-to-NO_2 conversion of powder mullite Sm(Y, Tb, Gd, Lu)Mn_2O_5 is evaluated by calculating the ratio between the produced NO_2 and the inlet NO, as shown in Figure 2. At the operating temperature of 300 °C, all the mullite oxides reach their maxima of catalytic activity in a sequence of $SmMn_2O_5$ > $LuMn_2O_5$ > YMn_2O_5 > $TbMn_2O_5$ > $GdMn_2O_5$. The $GdMn_2O_5$ and $LuMn_2O_5$ could act more effective in the temperature region from 150 °C to 200 °C. Arising from the small surface area

variations among these samples, the catalytic behaviour difference should stem from the intrinsic properties when A site elements are varied in mullite oxides A(Sm, Y, Tb, Gd, Lu)Mn_2O_5.

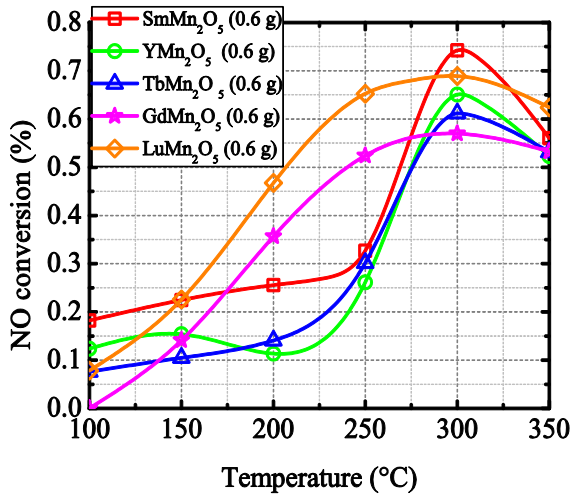

Fig. 2 NO conversion versus the ramping temperature for the Sm(Y, Tb, Gd, Lu)Mn_2O_5.

To identify the catalytic descriptor, inspired by previous pervoskite work in OR(E)R,[12] we investigate how the 3*d* electron occupation and the *p*-*d* hybridization between the O and Mn atoms impact catalytic activity of NO-to-NO_2 conversion. The DFT calculation is performed on a (2×1×1) unit cell as shown in Figure 3(a) to determine the 3*d* orbitals occupation of Mn_{oct} and Mn_{pyr}. The calculated average individual magnetic moments for Mn_{oct} and Mn_{pyr} are about 2.85 μ_B and 2.23 μ_B in AMn_2O_5 systems. For well-studied $TbMn_2O_5$, our simulation shows identical density of states (DOS) and projected density of states (PDOS) of Mn_{oct} and Mn_{pyr} (Figure 3(b)) comparing with previous reports.[16,17] And Sm(Y, Gd, Lu)Mn_2O_5 presents similar *d*-band shapes as $TbMn_2O_5$. To be more specific, in Figure 3(c), the ground-state high-spin configured Mn_{oct} and Mn_{pyr} could be regarded as t_{2g}^3 and ($d_{xz}^1, d_{yz}^1, d_{xy}^1, d_{z^2}^1$) respectively. The d_{z2} orbital has strong bonding with O-2*p* orbital in regards to t_{2g} orbitals. Thus, d_{z2}-band filling is crucial to govern the Mn-O* interaction. As the Fermi level locates above d_{z2} orbitals of Mn_{pyr} in Sm(Y, Tb, Gd, Lu)Mn_2O_5 oxides, thus the d_{z2} band fillings are all unit here (Figure 3(c)). This specific occupancy is superior for oxygen to interact with Mn on catalyst surfaces when either capturing or releasing external atomic O* (Figure 3(d)).[12]

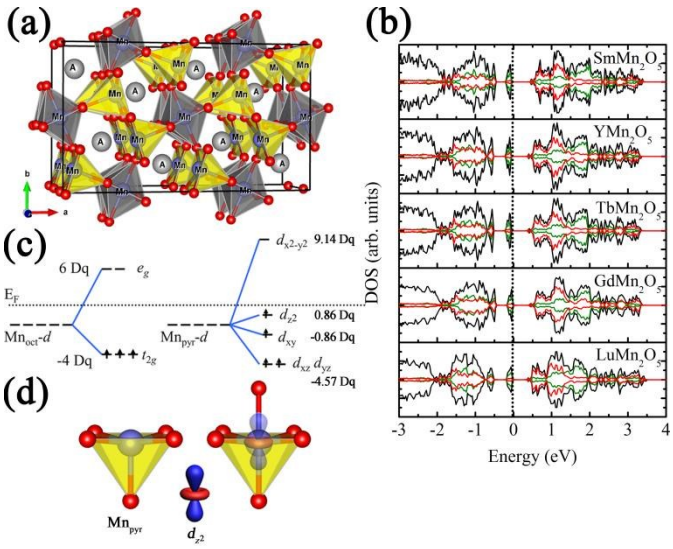

Fig. 3 (a) A 2 × 1 × 1 AMn_2O_5 unit cell. (b) the total and projected density of states of Sm(Y, Tb, Gd, Lu)Mn_2O_5. The E_F is set at zero energy. (c) the high-spin *d*-band configuration of the Mn_{oct} and Mn_{pyr} . (d) the square pyramid ligand field and the possible strong interaction between the O* and the d_{z2} orbital

Experimentally, the XAS Mn-*L* edge absorption spectra (Figure 4(a)) are obtained by measuring the transition from occupied Mn-2*p* core levels to the unoccupied 3*d* states, which is sensitive to the Mn valence. For different mullite Sm(Y, Tb, Gd, Lu)Mn_2O_5, the normalized spectra exhibit similar shapes in Mn-L_3 peak, indicating same average Mn valence i.e. same *d*-band filling. Thus, in terms of the e_g filling or *d*-band occupation based on both DFT calculations and XAS spectra, the Sm(Y, Tb, Gd, Lu)Mn_2O_5 are supposed to present close performance in the NO conversion. However, according to the catalytic efficiency shown in Figure 2, the NO conversion differs when the A-site rare-earth atom is changed. Therefore, *d*-band filling might be insufficient to describe the catalytic difference among various Mn-based mullite with only A-site changing.

When transition metal is bonding with oxygen, sulfur, chlorine and etc, the pre-edge features in XAS O(S, Cl)-*K* edge spectra reflects the anion *p* orbitals character mixed in metal *d* orbitals.[13, 18-21] Thus, the *p*-*d* hybridization which demonstrates the wavefunction overlap between the Mn-3*d* and O_{bulk}-2*p* orbitals in the Sm(Y, Tb, Gd, Lu)Mn_2O_5 could be characterized by the O-*K* edge absorption spectra.[13] All the spectra are normalized to the O atomic absorption at ~560 eV. The broad peak from ~540 eV to ~555 eV is the excitation from O_{bulk}-1*s* to the A-*d* (A=Sm, Y, Tb, Gd, Lu) and O_{bulk}-2*p* hybrid orbitals. The pre-edge peaks (527 eV ~ 537 eV) are contributed by the transition from O_{bulk}-1*s* to the Mn-3*d* and O_{bulk}-2*p* hybrid orbitals. The *p*-*d* hybridization strength (β^2) could be quantified by the absorption intensity of the pre-edge region after subtract the linear background,[18,19] which could be illustrated by the following equation:

$$\left|\beta^2\right| \propto \frac{\text{Absorption}}{\text{hole}_{e_g} + \frac{1}{4}\text{hole}_{t_{2g}}} \quad (1)$$

in which the hole represents the ligand holes with corresponding symmetry.[19] As the *d*-orbital occupations (ligand hole amount) are same in Sm(Y, Tb, Gd, Lu)Mn_2O_5, the hybridization strength can be obtained by integrate the peaks area in the XAS spectra. In Figure 4(b), after normalized to 555 eV the absorption intensity at the pre-edge region decreases from 1.56, 1.49, 1.46 to 1.40, 1.36 in the sequence of $SmMn_2O_5$ > $LuMn_2O_5$ > YMn_2O_5 > $TbMn_2O_5$ > $GdMn_2O_5$. This observation is well consistent with the NO conversion efficiency (Figure 4(c)). The peak at around ~533 eV reveals the major difference in the absorption spectra, which is identified as the hybridized region of Mn_{oct}-e_g and O_{bulk}-2*p* according to the Gaussian fitting in Figure 4(d). The *d*-band splitting sequence is determined from the DFT calculation results (See Supplementary Information). The energy differences between the fitting peaks are quantified by splitting energy (evaluated by *Dq*) which results from the Mn-O bond length. In the range from 1.90 to 2.02 Å, the 10 *Dq* value varies from 2.6 to 2.0 eV.[22] As the average Mn-O bond length in Sm(Y, Tb, Gd, Lu)Mn_2O_5 is 1.92 Å, the 10 *Dq* value in our work is set to 2.5 eV and the calculated and fitted peak center difference (labelled as a-d in Figure 4(d)) is summarized in Table 1. As a result, such *p*-*d* hybridization could act as the catalytic descriptor for Mn-based mullite oxides.

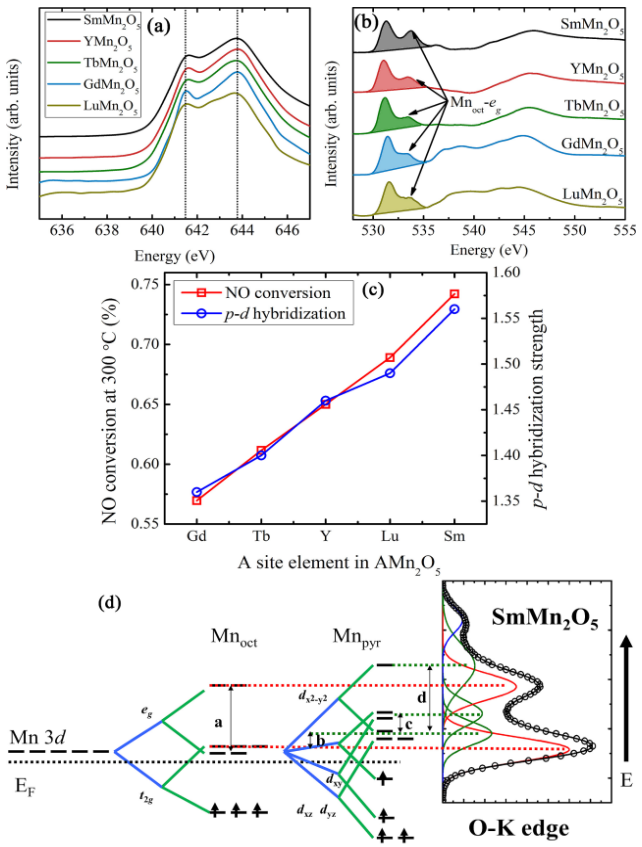

Fig. 4 Soft X-ray absorption (XAS) spectra of Sm(Y, Tb, Gd, Lu)Mn_2O_5. (a) XAS Mn-*L* edge absorption spectra, normalized to Mn-L_3 peak. (b) XAS O-*K* edge absorption. The shaded area represents the pre-edge and the peak around ~533 eV, which contribute by the Mn_{oct}-e_g orbitals, causes the major difference in absorption spectra. (c) The *p*-*d* hybridization strength versus the NO conversion rate. (d) Spin-splitting *d*-band alignment and the corresponding O-*K* edge XAS. The XAS spectra are Gaussian fitted and the fitted peak centers are verified by calcu- lating the ligand splitting energy in Table I.

Based on previous study, the NO conversion includes two steps, in which the O_2 would be firstly broken into two O* by Mn_{pyr}-Mn_{pyr} dimmer and then the NO would interact with one O* forming NO_2 molecule.[10] The rate limit step is formation of mono-dentate Mn-nitrate from the bi-dentate Mn-nitrate with an energy barrier of ~0.9 eV. During this elementary transition process, the key is how to release O* from Mn_{pyr} site to form mono-dentate Mn-nitrate and finally produce NO_2. Thus, a moderate O*-Mn_{pyr} bond strength is critical for the NO conversion.

Table 1. Calculated and fitted peak center differences labelled in Figure 4(d).

	Dq	Calculated (eV)	Fitted (eV)
a	10	2.50	2.63
b	3.1	0.78	0.73
c	4.6	1.15	1.03
d	13.7	3.43	2.96

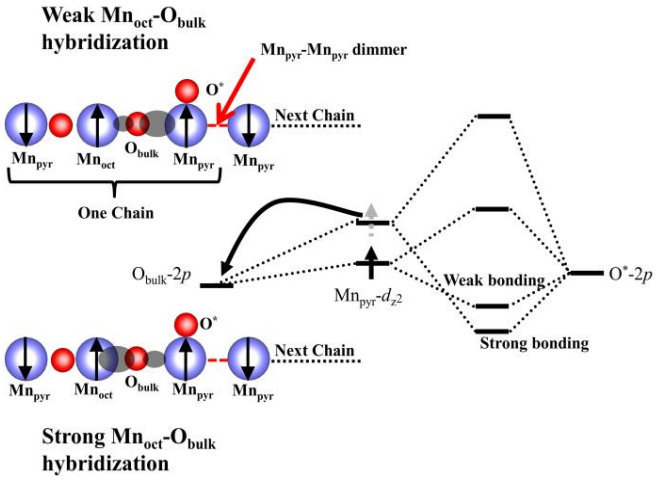

Fig. 5 Schematic diagram of the connection between the Mn_{oct}-3*d* and O_{bulk}-2*p* hybridization and the desorption of the O*. The energy of the d_{z^2} orbital could be modulated by the hybridization between Mn_{oct}-3*d* and O_{bulk}-2*p*, which consequently results in tunable bonding strength between Mn_{pyr} and O*.

As schematically shown in Figure 5, we proposed the mechanism how the external O* reaction with Mn_{pyr} is impacted by the Mn_{oct}-3*d* hybridizing with its neighbor bulk O- 2*p* when A site element differs. In the mullite crystal structure Mn_{oct} and Mn_{pyr} are in a chain of $Mn^{\uparrow}_{pyr} - O_{bulk} - Mn^{\uparrow}_{oct} - O_{bulk} - Mn^{\downarrow}_{pyr}$ along *b* direction (See Supplementary Information) Figure S2). The Mn_{pyr}-Mn_{pyr} dimmer which breaks the O_2 molecule into O* is formed by the neighboured Mn_{pyr} ions in two continuous chains (Figure 5). Especially, the electrons could hop within the sub-chain of $Mn^{\uparrow}_{pyr} - O_{bulk} - Mn^{\uparrow}_{oct}$ without violating Hund's rule.[23] As

an electronegative center, the O_{bulk} between the $Mn^{\uparrow}_{pyr}$ and $Mn^{\uparrow}_{oct}$ attracts electrons from both sides and the Mn covalence is largely influenced by Mn_{oct}-3*d* and O_{bulk}-2*p* hybridization.[24] Thus the hybridization between the O_{bulk} and the $Mn^{\uparrow}_{oct}$ here will strongly influence the electronic properties of $Mn^{\uparrow}_{pyr}$ due to the close connection between these two Mn ions. In XAS O-K edge absorption spectra, a relative weak intensity in Mn_{oct}-3*d*-e_g peak implies weak hybridization between Mn_{oct}-3*d* and O_{bulk}-2*p*. In such a way, the electrons become more localized on the Mn_{oct} atoms and the O_{bulk}-2*p* has more overlap with the Mn_{pyr} to compensate. Consequently the electron on the d_{z2} orbital (Mn_{pyr}) which is closest to the E_F (See Figure 3(d)) would be drained leading to the energy lifting of the d_{z2} orbital. As the d_{z2} orbital strongly interact with O*-2*p* orbitals, such energy lifting could result in the increase of the bonding strength between O* and Mn_{pyr} as shown in Figure 5, increasing the difficulty to release O*. Oppositely, when the hybridization between Mn_{oct}-3*d* and O_{bulk}-2*p* is strong, the electrons are more iterant and the interaction within the O* and Mn_{pyr} turns to be weaker. The weak O*-Mn_{pyr} bonding helps the catalyst surface to readily release O* and essentially form NO_2(g). Thus, to further enhance the active behaviour of the mullite-based catalyst, it is critical to refine the *p-d* hybridization strength between Mn_{oct} (Mn_{pyr}) and O_{bulk} (O*) through doping more (less) reactive elements in the period table. Specifically, doping on Mn_{oct}-site with more reactive 4+ elements (Mn's left in the transition region of the period table) results in the less bonding strength between Mn_{pyr} and O*. And the same goal could be obtained via direct doping Mn_{pyr} with less reactive 3+ elements (Mn's right or down in the transition region of the period table).

4 Conclusions

In conclusion, we claim that the *p-d* hybridization between the O_{bulk} and the Mn_{oct} could be a proper descriptor in predicting the catalytic activity of Mn-based mullite oxides (AMn_2O_5) in NO-to-NO_2 conversion. A more active performance could be expected through doping Mn_{oct} and Mn_{pyr} sites and essentially refining *p-d* hybridization strength between O*-Mn_{pyr}. The moderate O*-Mn_{pyr} bonding strength, stemming from the unit d_{z2} orbital filling and right *p-d* hybridization, could be potentially promising for OR(E)R reactions for the applications of water-splitting, fuel cell, Li-air batteries design and etc.

Acknowledgements

This work is supported by 1000 Youth Talents Plan, National Natural Science Foundation of China (11304161, 11104148, 51171082 and 11404172), Tianjin Natural Science Foundation (13JCYBJC41100, 14JCZDJC37700), the National Basic Research Program of China (973 Program with No. 2014CB931703). We thank the technology support from the Texas Advanced Computing Center (TACC) at the University of Texas at Austin (http://www.tacc.utexas.edu) for providing grid resources that have contributed to the research results reported within this paper. We thank Prof. Wanli Yang (Berkeley National Lab) for inspiration and useful discussions.

References

1 G. Ban-Weiss, J. P. McLaughlin, R. A. Harley, M. M. Lunden, T. W. Kirchstetter, A. J. Kean, A. W. Strawa, E. D. Stevenson and G. R. Kendall, *Atmospheric Environment*, 2008, **42,** 220-232
2 C. A. Pope III, *Aerosol Science and Technology* 2000, **32,** 4-14.
3 M. Shelef, *Chem. Rev.*, 1995, **95,** 209-225.
4 M. Koebel, G. Madia and M. Elsener, *Cata. Today*, 2002, **73,** 239.
5 A. M. Beale, F. Gao, I. Lezcano-Gonzalez, C. H. F. Peden and J. Szanyi, *Chem. Soc. Rev.*, 2015, (Advance article) DOI: 10.1039/C5CS00108K.
6 C. Wu, D. Schmidta, C. Wolvertonb and W. Schneidera, *J. Catal*., 2012, **286,** 88-94.
7 C. Kim, G. Qi, K. Dahlberg and W. Li, *Science*, 2010, **327,** 1624-1627.
8 Y. Wen, C. Zhang, H. He, Y. Yu and Y. Teraoka, *Catal.Today*, 2007, **126,** 400-405.
9 W. Epling, J. Parks, G. Campbell, A. Yezerets, N. Currier and L. Campbell, *Catal. Today*, 2004, **96,** 21-30.
10 W. Wang, G. McCool, N. Kapur, G. Yuan, B. Shan, M. Nguyen, U. M. Graham, B. Davis, G. Jacobs, K. Cho and X. Hao, *Science*, 2012, **337,** 832-835.
11 B. Hammer and J. K. Nørskov, *Advances in Catalysis.*, 2000, **45,** 71-129.
12 J. O. Bockris, T. Otagawa, *J. Electrochem. Soc.*, 1984, **131,** 290-302.
13 J. Suntivich, H. A. Gasteiger, N. Yabuuchi, H. Nakanishi, J. B. Goodenough and S.-H. Yang, *Nat. Chem.*, 2011, **3,** 546-550.
14 J. P. Perdew, K. Burke and M. Ernzerhof, *Phys. Rev. Lett.*, 1996, **77,** 3865.
15 Please refer to the link for the details of pseudopotential of *f*-elements "http://cms.mpi.univie.ac.at/vasp/vasp/_elements_I.html"
16 C. Wang, G.-C. Guo and L. He, *Phys. Rev. Lett.*, 2007, **99,** 177202.
17 T. -R. Chang, H.-T. Jeng, C.-Y. Ren and C.-S. Hsue, *Phys. Rev. B*, 2011, **84,** 024421.
18 F.M.F. deGroot, M. Gnom and J. C. Fuggle, *Phys. Rev. B*, 1989, **40,** 5715-5723.
19 M. Medarde, C. Dallera, M. Grioni, J. Voigt, A. Podlesnyak, E. Pomjakushina, K. Conder, Th. Neisius, O. Tjernberg and S. N. Barilo, *Phys. Rev. B*, 2006, **73**, 054424.
20 Y. Ha, A. L. Tenderholt, Richard H. Holm, B. Hedman, K. O. Hodgson and E. I. Solomon, J. Am. Chem. Soc., 2014, **136**, 9094-9105.
21 M. W. Löble, J. M. Keith, A. B. Altman, S. C. E. Stieber, E. R. Batista, K. S. Boland, S. D. Conradson, D. L. Clark, J. L. Pacheco, S. A. Kozimor, R. L. Martin, S. G. Minasian, A. C. Olson, B. L. Scott, D. K. Shuh, T. Tyliszczak, M. P. Wilkerson and R. A. Zehnder, J. Am. Chem. Soc., 2015, **137**, 2506-2523.
22 Y. Tanabe and S. Sugano, *J. Phys. Soc. Jpn.*, 1954, **9,** 766-779.
23 D. V. Efremov, J. Brink and D. I. Khomskii, *Nat. Mater.*, 2004, **3,** 853-856.
24 G. Giovannetti and J. Brink, *Phys. Rev. Lett.*, 2008, **100,** 227603.